

# DC and AC transport properties on $\text{La}_{0.8}\text{Sr}_{0.2}\text{MnO}_3$

Zhantao Wei · Xinsheng Yang · Li Lv ·  
Min Zhang · Yong Zhang

Received: 26 October 2013 / Revised: 25 March 2014 / Accepted: 28 March 2014 / Published online: 19 April 2014  
© The Author(s) 2014. This article is published with open access at Springerlink.com

**Abstract** Magnetoresistive sensor can be widely used in modern transportation field, such as the vehicle positioning and navigation system, vehicle detection system, and intelligent transportation system. In order to improve the efficiency of magnetoresistive sensor, we synthesized  $\text{La}_{0.8}\text{Sr}_{0.2}\text{MnO}_3$  polycrystalline bulks at different sintering temperatures and investigated their DC and AC transport properties in this work. As a result, all samples showed insulator–metal (I–M) phase transition, and the transition temperature ( $T_{\text{I–M}}$ ) shifted to higher temperature with the increase of sintering temperature. The  $T_{\text{I–M}}$  measured at different AC frequencies was smaller than that measured at DC condition, which implied that the I–M phase transition was suppressed at AC frequencies. The resistivity measured at high AC frequencies was larger than that measured at low AC frequencies, which could be attributed to the change of the magnetic penetration depth ( $\delta$ ). However, the room-temperature AC-magnetoresistance (MR) at low frequencies was much larger than that at high frequencies and room-temperature DC-MR. These findings demonstrate that reducing the AC frequency is an effective way for enhancing the room-temperature MR, which can be used to promote the efficiency of magnetoresistive sensor.

**Keywords** Magnetoresistance · Perovskite manganese oxides · DC and AC transport properties

## 1 Introduction

Magnetoresistance sensor, as one of the most active magnetic sensor technologies, which is widely applied in the vehicle positioning and navigation system, vehicle detection system, green transport systems, and so on [1]. Therefore, how to improve the efficiency of magnetoresistance sensor has been one of hot topics in these fields.

Since the discovery of colossal magnetoresistance (CMR) in perovskite manganese oxides with formula  $\text{L}_{1-x}\text{A}_x\text{MnO}_3$  (where L is a trivalent rare earth, and A is a divalent alkaline earth ion), many efforts have been devoted to integrate its transport properties and physical mechanisms, such as Jahn–Teller effect [2], double exchange [2, 3], phase separation [4], and charge order [5]. Meanwhile, lots of novel physical phenomena, such as spin glass behavior [6, 7] and exchange bias [8], were discovered. These findings indicated that  $\text{L}_{1-x}\text{A}_x\text{MnO}_3$  can be used in magnetoresistive sensor for improving the efficiency [9]. However, CMR effect is sensitive to temperature and only appears in the vicinity of the Curie temperature in a relative high magnetic field. This seriously limits the efficiency and application of magnetoresistive sensor. Thus, finding new ways to improve the room-temperature magnetoresistance (MR) in a low magnetic field become a hot topic, and many studies have been focused on it. It was found that introducing a second phase into the matrix is an effective way to improve magnetoresistance [10]. Gupta et al. [11] found that using Mo to substitute the Mn of  $\text{La}_{0.67}\text{Sr}_{0.33}\text{MnO}_3$  led to an enhancement of room-temperature MR. Many attempts have been made to study its AC transport properties which were measured with radio frequency ( $f > 1$  MHz). Rebello and Mahendiran [12] showed that the value of the AC-MR at room temperature in  $\text{La}_{0.7}\text{Sr}_{0.3}\text{MnO}_3$  is extremely high

---

Z. Wei · X. Yang · L. Lv · M. Zhang · Y. Zhang  
Key Laboratory of Magnetic Levitation Technologies and  
Maglev Trains, Ministry of Education of China, Chengdu  
610031, China

Z. Wei · X. Yang (✉) · L. Lv · M. Zhang · Y. Zhang  
Superconductivity and New Energy R&D Center, Southwest  
Jiaotong University, Chengdu 610031, China  
e-mail: xsyang@swjtu.edu.cn

( $\approx 47\%$  in a magnetic field where the magnetic induction intensity  $B = 0.1$  T and  $f = 3\text{--}5$  MHz). Aparnadevi and Mahendiran [13] revealed that the frequency dependent magnetotransport properties are dominated by the field and frequency dependence of AC permeability. However, the detailed AC transport properties of  $\text{La}_{0.8}\text{Sr}_{0.2}\text{MnO}_3$  at frequency less than 1 MHz have not been investigated.

In this work, a systematic study of AC electrical transport in the frequency range  $f = 0\text{--}14$  kHz based on the  $\text{La}_{0.8}\text{Sr}_{0.2}\text{MnO}_3$  was made. Their DC and AC transport properties were also presented. The room-temperature AC-MR at low frequencies is much larger than that at high frequencies and room-temperature DC-MR, which can be used to promote the efficiency of magnetoresistive sensor.

## 2 Experimental

$\text{La}_{0.8}\text{Sr}_{0.2}\text{MnO}_3$  polycrystalline bulks were prepared by sol-gel method, as elaborated in [10]. The obtained powers were carefully ground and pressed into wafers. Then, the wafers were sintered at various temperatures of 600, 800, 1,000, and 1,200 °C.

The phase structure and morphology were analyzed by X-ray diffractometer (XRD, X'Pert Panalytical) and field emission scanning electron microscope (FESEM, JSM-7001F), respectively. The DC and AC transport measurements were performed using electrical properties measurement system (ET-9000) with a lock-in amplifier (SR830) by the standard four-probe method. To insure the constant current measurement, a large resistor with a resistance 1,000 times higher than the value of samples was applied in the AC transport measurement.

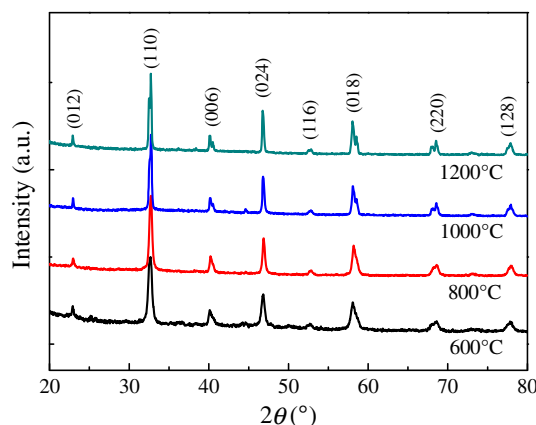
## 3 Results and discussion

Figure 1 shows XRD patterns of all samples. No peaks of other impurities are found under instrumental resolution, confirming that the product is composed of pure  $\text{La}_{0.8}\text{Sr}_{0.2}\text{MnO}_3$ . The strength of the major peak increases gradually as the sintering temperature rises. It is known that the average grain size of unit cell is characterized by Scherrer equation [8]:  $D \sim K\lambda/\beta\cos\theta$ , where  $K$  is the shape factor,  $\lambda$  is the wavelength of X-ray,  $\beta$  is the full width at half maximum (FWHM), and  $\theta$  is the diffraction angle. The average grain size, lattice parameters ( $a$ ,  $c$ ), and cell volume are calculated, as shown in Table 1. Obviously, with the sintering temperature increasing, the lattice parameter  $a$  decreases gradually, while the lattice parameter  $c$  increases. Moreover, the average grain size also increases with the increase of sintering temperature, which could be explained by the cluster effect [14]. Typical

FESEM images of all samples with different sintering temperatures are shown in Fig. 2. It can be seen that the grain size increases with the sintering temperature.

The DC resistivity was measured as a function of temperature ( $\rho\text{--}T$ ), as shown in Fig. 3. All samples exhibit the insulation-metal (I–M) phase transition, and the transition temperature ( $T_{\text{I-M}}$ ) shifts to high temperature regions as the sintering temperature increases. However, when a low magnetic field ( $B = 0.3$  T) is applied, the  $T_{\text{I-M}}$  shifts to low temperature regions, which could be confirmed by Fig. 5a. The resistivity decreases monotonously as the sintering temperature increases because of the decrease of grain boundaries [15]. It is obvious that the resistivity of the samples sintered at 600 °C is larger than that of other samples. The reason may lie in that there are a large number of magnetic disorders and amorphous grain boundaries in the samples sintered at 600 °C, which lead to the electrons receiving more scattering than that in other samples [16]. However, it is found that the room-temperature MR at 0.3 T is small, which limits its application in magnetoresistive sensor.

Furthermore, the  $\rho\text{--}T$  behaviors of  $\text{La}_{0.8}\text{Sr}_{0.2}\text{MnO}_3$  polycrystalline samples at different AC frequencies were measured, as shown in Fig. 4. All samples exhibit a similar trend as the temperature increases at AC frequencies varying from 0.133 to 13.333 kHz. All samples also have the I–M phase transition. It is noted that all curves show a flat range in the low frequency regions (133, 1,333 Hz) and then a gentle range in high frequency regions (3,333, 7,777, 13,333 Hz), which can be observed more clearly in samples with higher sintering temperature. It could be considered as an outcome of the classical skin effect. As the frequency of the alternative current increases, the flow of current is restricted to a specified thickness, which results in the increase of resistivity [17].



**Fig. 1** X-ray diffraction patterns of  $\text{La}_{0.8}\text{Sr}_{0.2}\text{MnO}_3$  polycrystalline bulks sintered at various temperatures

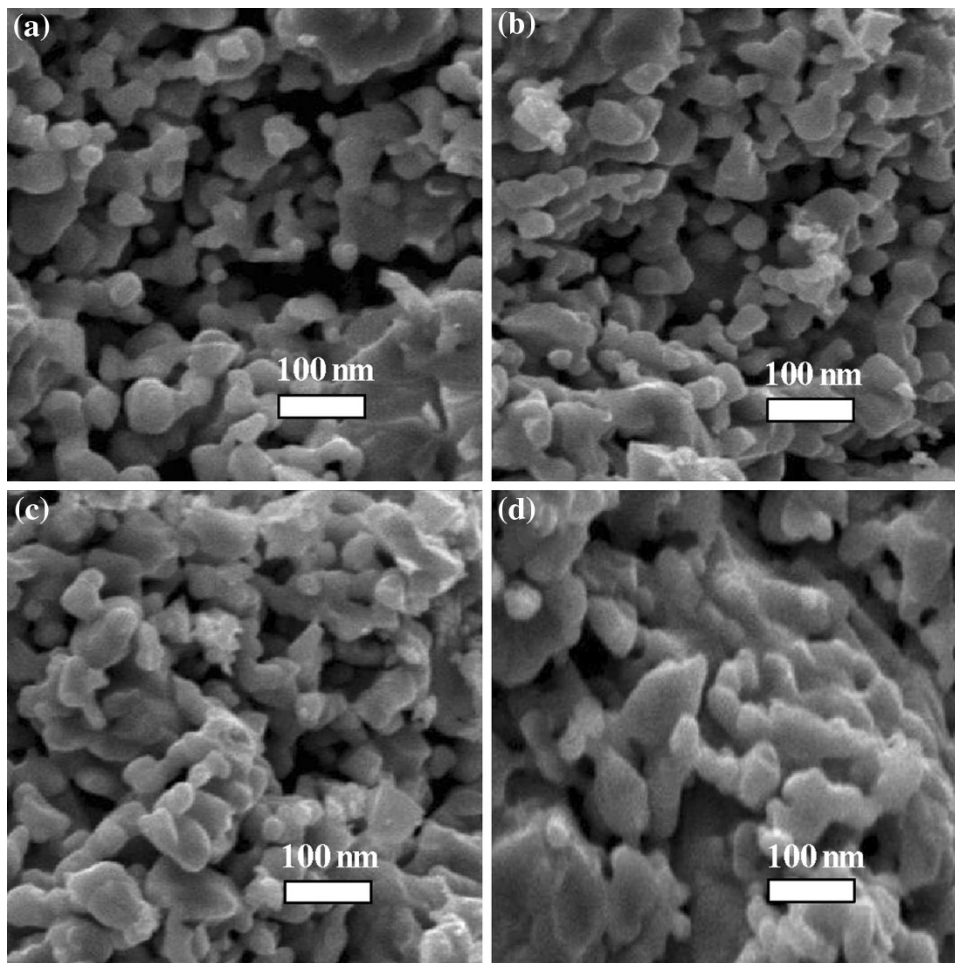
**Table 1** Structure parameters of samples sintered at different temperatures

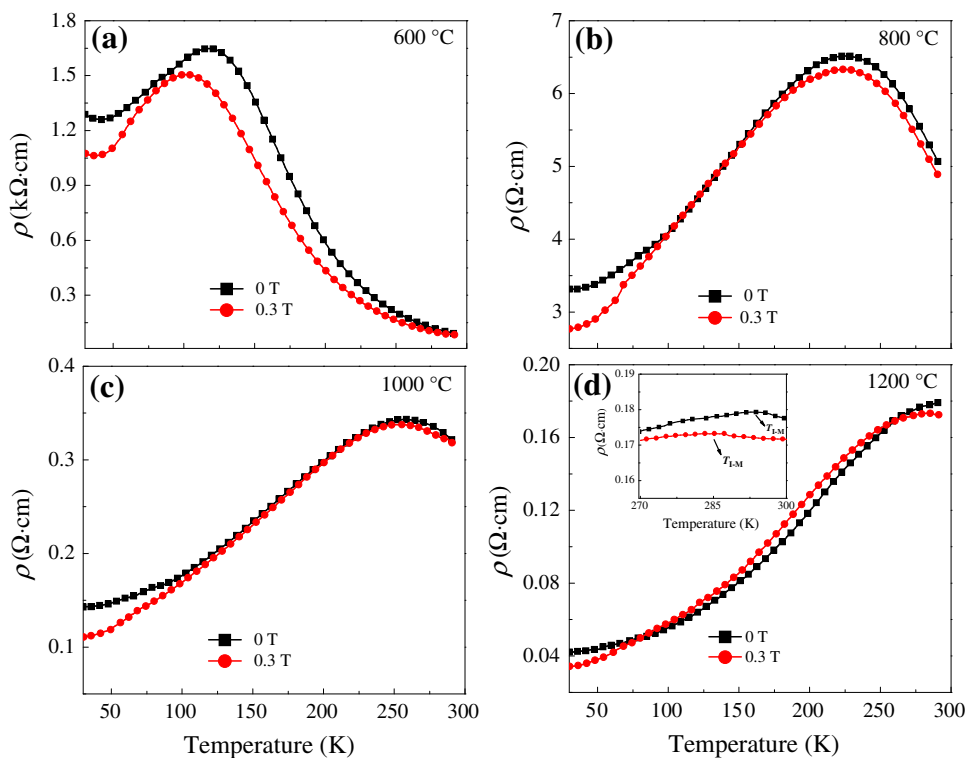
Sintering temperature (°C)	600	800	1,000	1,200
Average grain size (nm)	20	27	54	75
Lattice constant (Å)				
<i>a</i>	5.4970	5.4916	5.4749	5.4512
<i>c</i>	13.3739	13.3943	13.4299	13.4586
Cell volume (Å <sup>3</sup> )	349.967	349.605	348.613	347.082

Figure 5a shows the sintering temperature dependent  $T_{I-M}$  of samples measured at DC frequency in different applied magnetic fields. Obviously, the applied magnetic field leads to the decrease of  $T_{I-M}$ , and the  $T_{I-M}$  increases as the sintering temperature increases under 0 and 0.3 T. According to Dutta et al. [16], the sample with lower sintering temperature has a higher density of grain-boundary, which could scatter the electrons and then cause the

increase of resistivity. Naturally, lower value of  $T_{I-M}$  appears due to a stronger inhibitory effect from grain-boundary in the samples with lower sintering temperature. The frequency dependent  $T_{I-M}$  of samples at AC frequency in zero magnetic fields is shown in Fig. 5b. With frequency increasing,  $T_{I-M}$  first increases, reaching a maximum, and then decreases. The  $T_{I-M}$  measured at different AC frequencies is smaller than that measured at DC condition, which implies that the I–M phase transition is suppressed at AC frequencies.

In order to study in detail the influence of frequency on resistivity, we define the resistance change rate at different frequencies as  $\Delta\rho/\rho(0) = (\rho(f) - \rho(0))/\rho(0)$ , where the  $\rho(f)$  is the resistance obtained at different AC frequencies in zero DC magnetic field, and  $\rho(0)$  is the resistance obtained at  $f = 0$  Hz. Figure 6 shows the temperature dependent  $\Delta\rho/\rho(0)$  of all samples measured at low frequencies ( $f = 133, 1,333$  Hz) in zero DC magnetic field. Obviously, all samples show a peak near the  $T_{I-M}$  in  $\Delta\rho/\rho(0)$  versus  $T$  curve. This phenomenon is similar to the

**Fig. 2** Typical FE–SEM images of samples with different sintering temperature. **a** 600 °C. **b** 800 °C. **c** 1,000 °C. **d** 1,200 °C



**Fig. 3** Temperature dependent resistivity in different applied magnetic fields for samples sintered at different temperatures. **a** 600 °C. **b** 800 °C. **c** 1,000 °C. **d** 1,200 °C. Inset in **(d)** transition temperature  $T_{I-M}$  of sample sintered at 1,200 °C

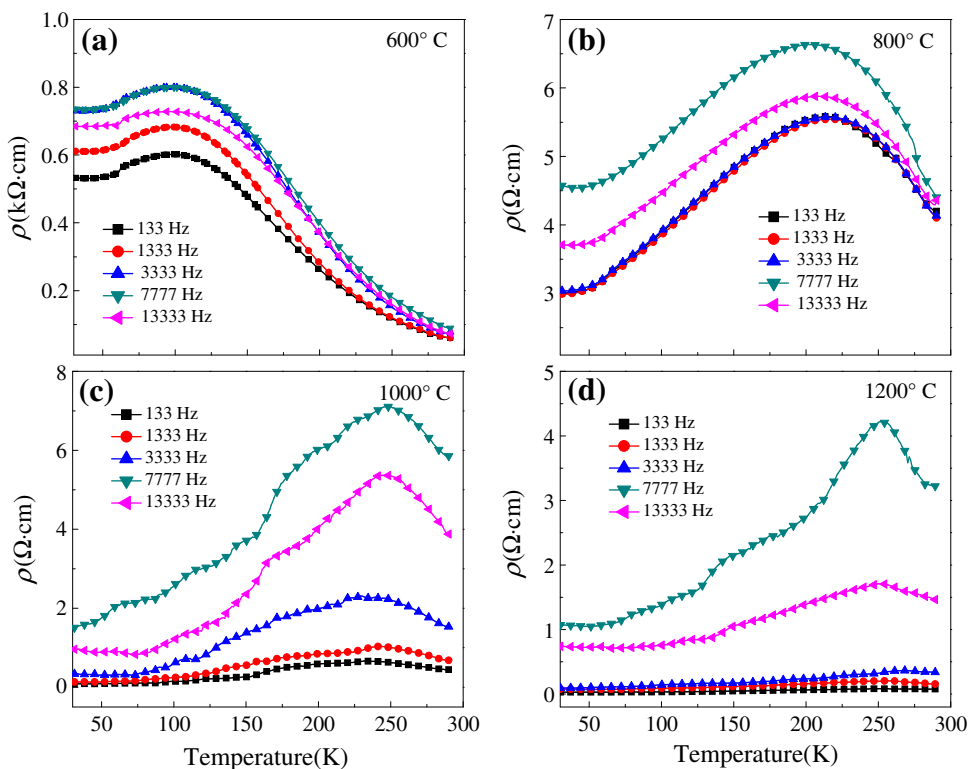


**Fig. 4** Temperature dependent resistivity at different AC frequencies in zero magnetic field for all samples sintered at different temperatures. **a** 600 °C. **b** 800 °C. **c** 1,000 °C. **d** 1,200 °C

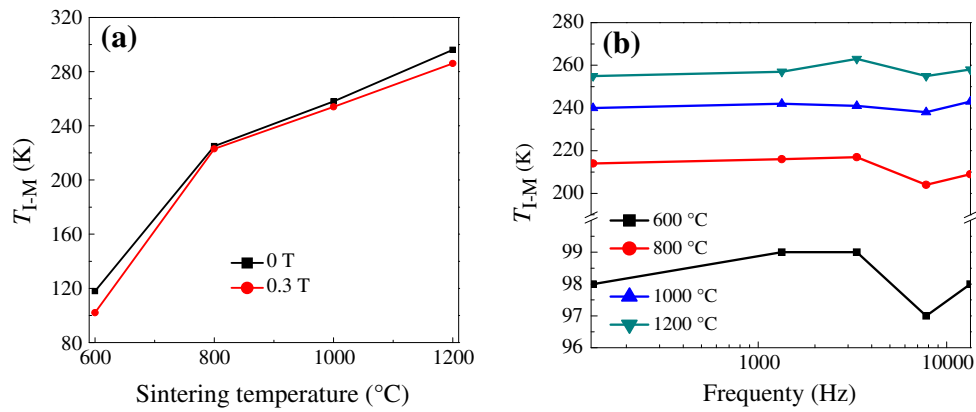


**Fig. 5** Sintering temperature dependent  $T_{I-M}$  of samples at DC frequency in different applied magnetic fields (a) and frequency dependent  $T_{I-M}$  of samples at AC frequency in zero applied magnetic field (b)

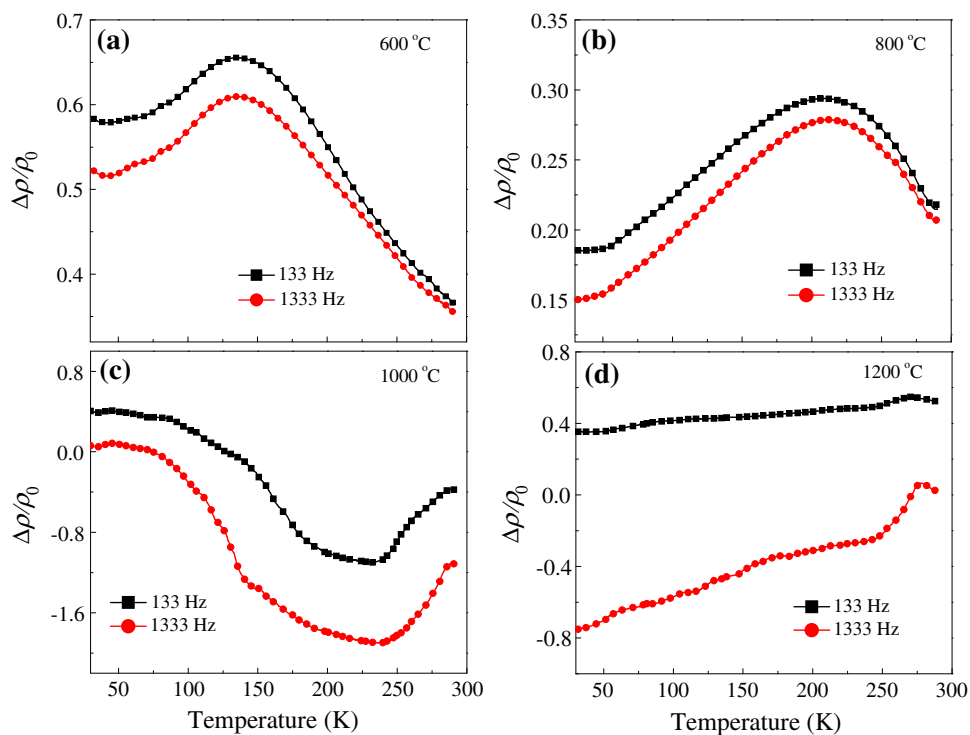


**Fig. 6** Temperature dependent  $\Delta\rho/\rho(0)$  at low frequencies ( $f = 133$  Hz, 1,333 Hz) in zero DC magnetic field for samples sintered at different temperatures. **a** 600 °C. **b** 800 °C. **c** 1,000 °C. **d** 1,200 °C

intrinsic magneto-resistance peak, which could be due to the magnetic domains and strain free structure [18]. The features may be explained by the fact that the change of AC frequency causes a induce magnetic field, and thus leads to the change of resistivity. Further theoretical research is required to fully understand its physical mechanism.

Figure 7 shows the AC-MR  $((\rho(H) - \rho(0))/\rho(0) \times 100 \%)$  as a function of frequency at 290 K under 0.3 T.

All samples exhibit a similar MR- $f$  behavior that is MR first increases, reaching a maximum, and then decreases. The MR measured at low frequencies is obviously larger than that measured at high frequencies, especially for the samples with higher sintering temperature. Obviously, the room-temperature AC-MR is largely enhanced compared with the room-temperature DC-MR (inset in Fig. 7). It provides a novel way to promote the sensitivity and efficiency of magnetoresistive sensor.

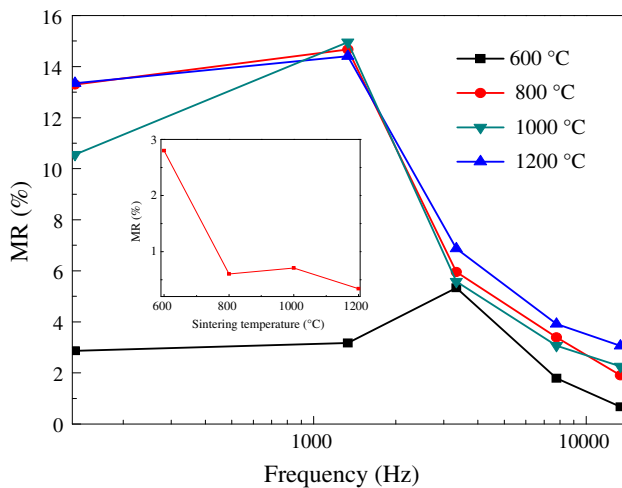


**Fig. 7** Frequency dependence of AC-MR of all samples under 0.3 T at 290 K. *Inset* DC-MR at 290 K as a function of sintering temperature

#### 4 Conclusion

The detailed AC and DC transport properties of  $\text{La}_{0.8}\text{Sr}_{0.2}\text{MnO}_3$  polycrystalline samples have been studied. All samples show the I–M phase transition in both DC and AC measurements. The  $T_{I-M}$  measured at different AC frequencies is smaller than that measured at DC condition, which implies that the I–M phase transition is suppressed by AC frequency. The resistivity at high AC frequencies is obviously larger than that at low AC frequencies. However, the room-temperature AC-MR at low frequencies is much larger than that at high frequencies and room-temperature DC-MR. These findings provide an alternative strategy to probe the spin-charge coupling in manganites and open a huge potential application prospect in modern intelligent transportation field.

**Acknowledgments** This work was supported by the National Magnetic Confinement Fusion Science Program (No. 2011GB112001), Program of International S&T Cooperation (No. 2013DFA51050), the National Natural Science Foundation of China (Nos. 51002125, 11104224, 11004162, and 51271155), the Research Fund for the Doctoral Program of Higher Education of China (No. 20110184120029), the Fundamental Research Funds for the Central Universities (Nos. 2682013ZT16, SWJTU12CX18, SWJTU11ZT31, 2682013CX004, and SWJTU11BR063), and the Science Foundation of Sichuan Province (Nos. 2011JY0031 and 2011JY0130).

**Open Access** This article is distributed under the terms of the Creative Commons Attribution License which permits any use, distribution, and reproduction in any medium, provided the original author(s) and the source are credited.

#### References

1. Taghvaeeyan S, Rajamani R (2011) Use of vehicle magnetic signatures for position estimation. *Appl Phys Lett* 99(13):134101-134101-3
2. Hrabovský D, Caicedo JM, Herranz G et al (2009) Jahn–Teller contribution to the magneto-optical effect in thin-film ferromagnetic manganites. *Phys Rev B* 79(5):052401
3. Gu M, Song C, Yang F et al (2012) Tuning magnetic and transport properties through strain engineering in  $\text{La}_{0.7}\text{Sr}_{0.3}\text{MnO}_3/\text{La}_{0.5}\text{Sr}_{0.5}\text{TiO}_3$  superlattices. *J Appl Phys* 111(8):084906-084906-6
4. Saber MM, Egilmez M, Schoofs F et al (2012) Strain, spin disorder, and thickness dependence of magneto-transport in  $\text{Sm}_{0.55}\text{Sr}_{0.45}\text{MnO}_3$  films. *Appl Phys Lett* 100(25):252408-252408-5
5. Hu L, Sheng Z, Hu X et al (2012) Control of the charge/orbital ordering transition in epitaxial  $\text{La}_{7/8}\text{Sr}_{1/8}\text{MnO}_3$  thin films through compressive strain. *J Phys D Appl Phys* 45(17):175002
6. Wang KF, Wang Y, Wang LF et al (2006) Ferromagnetic metal to cluster-glass insulator transition induced by A-site disorder in manganites. *Appl Phys Lett* 88(16):152505-152505-3
7. Rivadulla F, Lopez-Quintela MA, Rivas J (2004) Origin of the glassy magnetic interactions in  $\text{GdMe}_x\text{Mn}_{1-x}\text{O}_3$  perovskite (Me = transition metal). *Phys Rev Lett* 3:167206-167206-4
8. Qian T, Li G, Zhang T et al (2007) Exchange bias tuned by cooling field in phase separated  $\text{Y}_{0.2}\text{Ca}_{0.8}\text{MnO}_3$ . *Appl Phys Lett* 90(1):012503-012503-3
9. Daubaras A, Zilyus M (2012) Vehicle detection based on magneto-resistive magnetic field sensor. *Electron Electric Eng* 118(2): 27–32
10. Yang L, Yang X, Cheng C et al (2012) Structure and electrical properties in polymer bonded  $\text{La}_{0.7}\text{Sr}_{0.3}\text{MnO}_3$  composites. *Phys Procedia* 27:92–95
11. Gupta S, Ranjit R, Mitra C et al (2001) Enhanced room-temperature magnetoresistance in  $\text{La}_{0.7}\text{Sr}_{0.3}\text{MnO}_3$ -glass composites. *Appl Phys Lett* 78(3):362–364
12. Rebello A, Mahendiran R (2010) Influence of length and measurement geometry on magnetoimpedance in  $\text{La}_{0.7}\text{Sr}_{0.3}\text{MnO}_3$ . *Appl Phys Lett* 96(3):032502-032502-3
13. Aparnadevi M, Mahendiran R (2013) Alternating current magnetotransport in  $\text{Sm}_{0.1}\text{La}_{0.6}\text{Sr}_{0.3}\text{MnO}_3$ . *AIP Adv* 3(1):012114-012114-8
14. Djerdj I, Tonejc AM (2006) Structural investigations of nanocrystalline  $\text{TiO}_2$  samples. *J Alloys Compd* 1:159–174
15. Vazquez-Vazquez C, Blanco MC, Lopez-Quintela MA et al (1998) Characterization of  $\text{La}_{0.67}\text{Ca}_{0.33}\text{MnO}_3 \pm \delta$  particles prepared by the sol–gel route. *J Mater Chem* 8(4):991–1000
16. Anulekha Dutta, Gayathri N, Ranganathan R (2003) Effect of particle size on the magnetic and transport properties of  $\text{La}_{0.875}\text{Sr}_{0.125}\text{MnO}_3$ . *Phys Rev B* 68(5):054432
17. Naik VB, Rebello A, Mahendiran R (2009) A large magnetoinductance effect in  $\text{La}_{0.67}\text{Ba}_{0.33}\text{MnO}_3$ . *Appl Phys Lett* 95(8):082503-082503-3
18. Hwang HY, Cheong S-W, Ong NP et al (1996) Spin-polarized intergrain tunneling in  $\text{La}_{2/3}\text{Sr}_{1/3}\text{MnO}_3$ . *Phys Rev Lett* 77: 2041–2044